then lies in free space. The electric vector potential is

$$\overline{F} = \epsilon \frac{e^{-jkr}}{4\pi r} \int e^{jk\hat{r}\cdot\vec{r}'} \overline{M}(\vec{r}')\, d\vec{r}'$$

$$F_x = \epsilon \frac{e^{-jkr}}{4\pi r} 2t \left[\int_0^a e^{j\tilde{k}_x x'} \cos\left(\frac{m\pi x'}{a}\right) dx' - (-1)^n e^{j\tilde{k}_y b} \int_0^a e^{j\tilde{k}_x x'} \cos\left(\frac{m\pi x'}{a}\right) dx' \right]$$

$$= \epsilon \frac{e^{-jkr}}{4\pi r} 2t g_1(\theta, \phi)$$

$$F_y = -\epsilon \frac{e^{-jkr}}{4\pi r} 2t g_2(\theta, \phi)$$

in terms of which the electric far field is $\overline{E} = j\omega\eta\hat{r} \times \overline{F}$.

If the patch antenna is designed to operate at the lowest order mode, then $m = 0$ and $n = 1$. At $\theta = 0$,

$$g_2 \sim \int_0^b \cos\left(\frac{\pi y'}{b}\right) dy' = 0 \tag{3.65}$$

Added a factor of a in two equations 5/24/2019 kfw

so that the edges at $x = 0$ and $x = a$ do not radiate significantly. For the other edges,

$$g_1 = [1 - (-1)^1 e^{j\tilde{k}_y b}] \int_0^a \cos(0) e^{j\tilde{k}_x x'} dx'$$

$$= 2a e^{j\tilde{k}_y b/2} \cos(\tilde{k}_y b/2) \frac{e^{j\tilde{k}_x a} - 1}{j\tilde{k}_x a}$$

$$= 2a e^{j\tilde{k}_x a/2} e^{j\tilde{k}_y b/2} \cos(\tilde{k}_y b/2) \frac{\sin(\tilde{k}_x a/2)}{\tilde{k}_x a/2}$$

where $\tilde{k}_x = k \sin\theta \cos\phi$ and $\tilde{k}_y = k \sin\theta \sin\phi$. The directivity, radiation resistance, and other parameters can be found from the far electric field.

To estimate the directivity of the patch antenna, a patch operating in the fundamental mode can be modeled as two parallel, horizontal magnetic dipoles aligned with the two radiating edges of the patch. The directivity is the product of 3/2 for one dipole, a factor of two to account for both dipoles, and another factor of two to account for the ground plane and the one-sided radiation pattern, leading to a directivity of 6.

3.7 Aperture Antennas

Wire, loop, and patch antennas are excited by a transmission line. If the excitation is a propagating wave, instead of a transmission line, we refer to the antenna as an aperture antenna (Fig. 3.4). The propagating wave is typically produced by another transducer which is itself an antenna and provides the transmission line connection for the aperture antenna. Aperture antennas include the open-ended waveguide, slotted waveguide, horn antennas, and reflectors. The feed of a parabolic dish or other type of reflector antenna is often another aperture antenna such as an open-ended waveguide or horn.

Here, we round out the discussion of reflector antennas and give some practical information about types of reflectors, reflector geometry, achievable aperture efficiency, and a common method for modeling reflectors based on the physical optics approximation.

The most common reflector antenna is a paraboloid. The paraboloid has a single focal point and offers the highest directivity for a given aperture area. With symmetric paraboloidal reflector antennas, the feed antenna at the focal point and feed supports block some of the radiated field, leading to gain loss. An offset feed configuration can be used to reduce blockage. The reflector is an offset section of a parent paraboloid, with the feed at the focus of the parent paraboloid. The Green Bank Telescope has an unblocked aperture, and offset feeds are commonly used for satellite communication ground terminals.

In various applications, reflectors with spherical, cylindrical, elliptical, and other geometries are also used. Elliptical reflectors are used in ground based satellite communication systems to allow multiple feeds to form beams aimed at different geostationary satellites. Spherical reflectors are used for astronomical radio telescopes where the reflector must be fixed, and the feed is moved to steer the beam in different directions. An example is the Arecibo Observatory in Puerto Rico. The Chinese Five hundred meter Aperture Spherical Telescope (FAST) has a reflector surface that deforms using cables to produce a parabolic surface with movable focus. Cylindrical reflectors are used to produce a line focus, with the CHIME instrument as an example.

Reflectarrays and transmitarrays use passive elements, typically on a planar surface, with adjustable geometries or loading impedances, to produce reflection or transmission phase variations across the aperture that focus a wave without the curvature used in conventional reflector antennas.

Reflectors can be understood using a ray tracing or geometrical optics model. For a parabolic reflector, a spherical wave from a point source is transformed into a plane wave. Diffraction due to the finite size of the reflector causes the far-field pattern to consist of a narrow distribution of plane waves, so that the radiation pattern is a sinc-like function of angle from the reflector axis or boresight, referred to as an Airy function. As a receiver, a plane wave incident on a parabolic reflector focuses into a distribution that has an Airy function dependence on distance from the focus. From the feed to the reflector, a near to far transform takes place, and a second near to far transform occurs from the reflector to the far field. Consequently, there is a double Fourier transform from the focal plane to the far field, and the radiation pattern of a reflector antenna is qualitatively similar as a function of angle to the dependence of the focused field in the focal plane on distance from the focal point.

For a basic paraboloidal reflector, the key parameters are the focal length f and the diameter D. The ratio f/D is important, since that determines the angular extent of the reflector from the point of view of the feed. Large f/D corresponds to a shallow reflector, and a deep reflector has a small f/D. Dish designs for communications, radio astronomy, and satellite links commonly lie in the middle range with f/D values from 0.3 to 0.6.

One key tradeoff for reflector antennas involves the radiation pattern of the feed. For a small feed horn antenna with broad illumination pattern, both the aperture efficiency

4.1 The Array Factor and Classical Array Analysis

The basic method used in classical array analysis and synthesis is the array factor approximation. We will briefly derive the array factor here, and use it to develop basic results in the theory of the uniform linear array (ULA). We will consider the benefits and limitations of this approach, before moving to the network theory and pattern overlap integral formulation.

We will assume in this section that the array element radiation patterns are identical and that the elements differ only in their locations and driving excitation phase and magnitude. Nearly all arrays employ identical elements, so the assumption of identical elements is not a serious limitation. It is more significant that we will assume that the element radiation patterns are identical.

The critical assumption made here is that the radiation patterns of the elements in the array are identical. When an element is excited, the radiated fields induce currents on nearby elements, which produces an additional contribution to the radiated fields. The equivalent current for an element in an array has a large component on the driven element, and smaller components on the other elements around the driven elements. For elements near the edge of the array, the coupled currents are different because there are fewer nearby elements than is the case for elements in the interior of the array. Even though the elements in the array are identical, the elements in the array are effectively represented by different equivalent currents. This means that the embedded element radiation pattern (including radiation from currents induced on neighboring elements) is different from the radiation pattern of the antenna element in isolation. If coupling between elements can be neglected, or if the array is large, edge element effects are ignored, the assumption of identical element radiation patterns is valid and the array factor method considered here is applicable.

Consider an antenna located at the origin of the coordinate system and excited with a driving input current I_0 such that the antenna equivalent current source is $\overline{J}$. From the far-field radiation integral (2.13), we have for the radiated far field

$$\overline{E}_{\text{el}}(\overline{r}) = -j\omega\mu(1 - \hat{r}\hat{r}\cdot)\frac{e^{-jkr}}{4\pi r}\int d\overline{r}'\, e^{j\overline{k}\cdot\overline{r}'}\overline{J}(\overline{r}') \tag{4.1}$$

where $\overline{k} = k\hat{r}$. If the antenna is shifted from the origin to the point $\overline{r}_1$, the field becomes

Added cdots in three equations

$$\begin{aligned}\overline{E}_1(\overline{r}) &= -j\omega\mu(1 - \hat{r}\hat{r}\cdot)\frac{e^{-jkr}}{4\pi r}\int d\overline{r}'\, e^{j\overline{k}\cdot\overline{r}'}\overline{J}(\overline{r}' - \overline{r}_1) \\ &= -j\omega\mu(1 - \hat{r}\hat{r}\cdot)\frac{e^{-jkr}}{4\pi r}e^{j\overline{k}\cdot\overline{r}_1}\int d\overline{r}''\, e^{j\overline{k}\cdot\overline{r}''}\overline{J}(\overline{r}'') \\ &= e^{j\overline{k}\cdot\overline{r}_1}\overline{E}_{\text{el}}(\overline{r})\end{aligned} \tag{4.2}$$

This result indicates that a shift in the location of the antenna leads to a phase shift in the far field. This is essentially an application to a radiating current source of the Fourier shift theorem.

We will now use this result to combine the fields radiated by the elements in an antenna array. If we have an array of N identical elements driven with phasor excitation

$n > 1$ and $|x| > 1$, the magnitude increases without bound for orders above $n = 0$, since $\cos^{-1}(x)$ is imaginary. Several low order Chebyshev polynomials are shown in Fig. 4.2.

To use Chebyshev polynomials as an array factor, we need to transform from the far-field angle of the pattern to the argument x of the polynomials. We want $\pi/2$ to correspond to a value of x that is larger than one, in order to form the main lobe. Sidelobe angles should transform to $|x| \leq 1$. This is accomplished by the Dolph transformation

$$x = b\cos(u/2), \quad b > 1 \tag{4.32}$$

where $u = kd\cos\theta - \alpha$. For an N element array, the array factor that we want to obtain is

$$A(u) = T_{N-1}[x(u)] \tag{4.33}$$

where the degree of the Chebyshev polynomial is determined by the fact that an N element array corresponds to a polynomial in u of order $N - 1$. In order to realize this radiation pattern, we need to develop a procedure for determining array element excitations that produce an array factor given by (4.33).

With the array elements centered on $z = 0$, the array factor is

$$A(u) = \sum_{n=1}^{N/2} e^{j(n-1/2)u} i_n + \sum_{n=1}^{N/2} e^{-j(n-1/2)u} i_{-n}, \quad (N \text{ even})$$

$$A(u) = i_0 + \sum_{n=1}^{(N-1)/2} e^{jnu} i_n + \sum_{n=1}^{(N-1)/2} e^{-jnu} i_{-n}, \quad (N \text{ odd})$$

We will now assume that the excitations i_n are symmetric about $z = 0$, so that $i_{-n} = i_n$. By combining symmetric terms in the sums, the array factor can be expressed as

$$A(u) = 2\sum_{n=1}^{N/2} \cos[(n - 1/2)u] i_n, \quad (N \text{ even}) \tag{4.34a}$$

$$A(u) = i_0 + 2\sum_{n=1}^{(N-1)/2} \cos(nu) i_n, \quad (N \text{ odd}) \tag{4.34b}$$

For the even case, using the Dolph transformation,

$$A(u) = 2\sum_{n=1}^{N/2} \underbrace{\cos[(2n-1)\cos^{-1}(x/b)]}_{T_{2n-1}(x/b)} i_n = T_{N-1}(x) \tag{4.35}$$

so that designing the array requires finding excitations such that

$$2\sum_{n=1}^{N/2} T_{2n-1}(x/b) i_n = T_{N-1}(x) \tag{4.36}$$

A similar result is obtained for the case of N odd. This expression shows that designing the excitations for a Dolph–Chebyshev array requires that we express the order $N - 1$ Chebyshev polynomial as a linear combination of the polynomials of order 1, 3, 5, ..., $N - 1$ with argument scaled by $1/b$. The coefficients of the linear combination are the excitation currents.

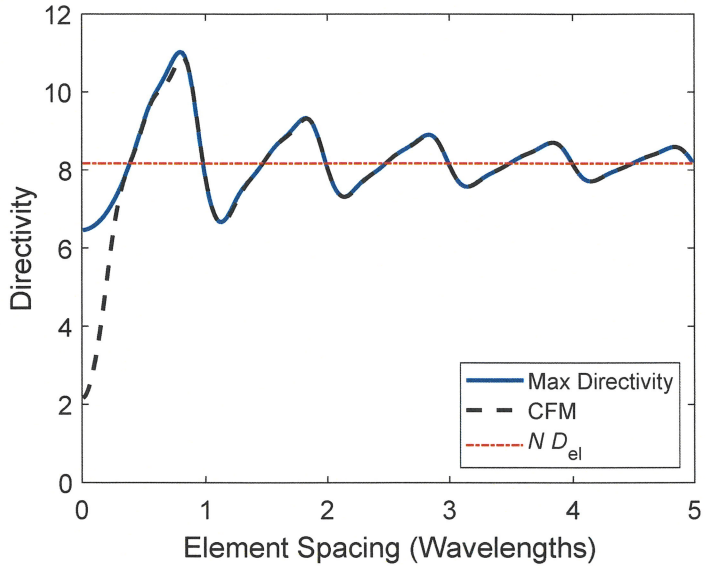

Figure 6.7 Directivity of a four element parallel half-wave dipole array as a function of element spacing.

included, the sensitivity of the array for a superdirective beamformer drops so that it is comparable to the sensitivity with the CFM beamformer, and the superdirectivity is rendered moot. In other words, the isotropic noise gain may be large, but the array gain is modest.

For the broadside beam, the maximum directivity at small element spacings is smaller than the limiting directivity at large spacings, whereas for a beam steered to endfire, the maximum directivity at small spacings is higher than the directivity at large element spacings.

Figure 6.7 - Removed K from the vertical axis label 5/20/2019

6.17 Summary

For a complex active receiving array system, the figures of merit considered in this chapter can be used in the design process to optimize the system, as well as in the engineering test and deployment phases to characterize the performance of the fabricated system. In the design phase, the receiver can be analyzed and optimized with the efficiency parameters considered in this chapter, by adjusting the element design, array configuration, and amplifier noise parameters to maximize the efficiencies and the overall system sensitivity.

Since the efficiency parameters depend on beamformer coefficients, the beamforming process must be considered together with the array element design. For an active array, the system cannot be as readily decoupled into separate antenna and electronics design problems as with a single-antenna receiver system. Consequently, optimizing highly

sensitive active array receivers requires a consideration of the full system, including beamforming, and the modeling and design of these systems poses many challenging and interesting engineering problems, some of which are treated in the following chapters.

Problems

6.1 For the dipole array of Problem 5.4, add receiver noise to the model. The front end low noise amplifiers have noise figure 2 dB, noise resistance $R_N = 15$ Ohms, and correlation admittance $Y_c = 0$. Assume that noise added by components after the LNAs is negligible. Compute the open circuit loaded receiver noise correlation matrix, isotropic external noise correlation matrix, and signal correlation matrix. Find the equivalent system noise temperature, receiver sensitivity, and the noise matching efficiency.

added period 5/24/2019 kfw

6.2 Using the model of Problem 6.1 for a four element parallel dipole array, find the (a) array gain with full noise model, (b) array gain with isotropic external noise only. (c) Compare these to the directivity of the array.

6.3 Consider the ULA of Problem 4.8 as a receive array. (a) Find the array weights which maximize the white noise array gain instead of the directivity. (b) Plot the maximum white noise gain on top of the gain curves as a function of element spacing from Problem 4.8. How is it that the white noise array gain can be higher than the maximum directivity for some array element spacings?

References

[1] P. W. Hannan, "The element-gain paradox for a phased-array antenna," IEEE Trans. Antennas Propag., vol. 12, no. 4, pp. 423–433, Jul. 1964.

[2] *IEEE Standard Definitions of Terms for Antennas*, IEEE Std 145-2013.

[3] K. F. Warnick, M. V. Ivashina, R. Maaskant, and B. Woestenburg, "Unified definitions of efficiencies and system noise temperature for receiving antenna arrays," IEEE Trans. Antennas Propag., vol. 58, no. 6, pp. 2121–2125, 2009.

[4] K. F. Warnick and B. D. Jeffs, "Gain and aperture efficiency for a reflector antenna with an array feed," IEEE Antennas and Wireless Propagation Letters, vol. 5, p. 499, 2006.

[5] M. V. Ivashina, R. Maaskant, and B. Woestenburg, "Equivalent system representation to model the beam sensitivity of receiving antenna arrays," IEEE Antennas and Wireless Propagation Letters, vol. 7, no. 1, pp. 733–737, 2008.

[6] E. E. M. Woestenburg and K. F. Dijkstra, "Noise characterization of a phased array tile," in *Proc. European Microwave Conference*, vol. 33, Munich, Germany, 2003, pp. 363–366.

[7] E. E. M. Woestenburg and J. C. Kuenen, "Low noise performance perspectives of wideband aperture phased arrays," in *The Square Kilometre Array: An Engineering Perspective*, Springer, 2005, pp. 89–99.

dependent on the f/D ratio of the reflector antenna, and weakly dependent on the feed pattern. As seen in Fig. 7.10, the maximum number of high-performance off-axis beams is very limited for deep reflectors (where the f/D ratio is smaller than 0.5) and is almost the same number for the horn feeds having a relative illumination taper at the reflector rims in the range of −6 to −12 dB.

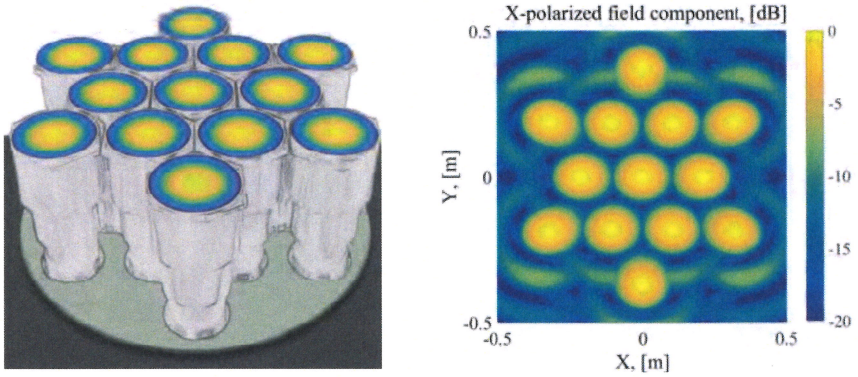

(a) (b)

Figure 7.9 Illustration of the focal field mismatch and under-sampling effects for conventional cluster feeds in one-horn-per-beam configuration: (a) typical aperture field distributions of individual horns in the cluster feed; and (b) reflector focal field distributions for the corresponding plane waves incident from multiple directions (reflector f/D ratio is 0.35).

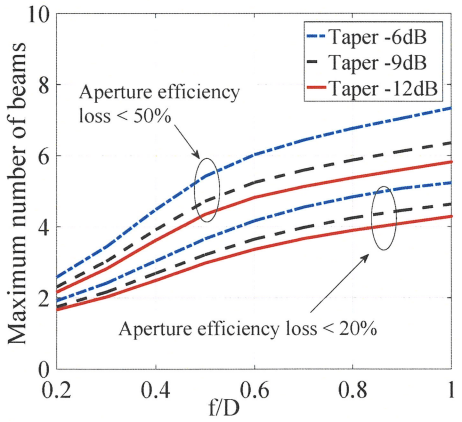

Figure 7.10 Maximum number of high-efficiency off-axis beams that can be generated by a cluster feed of horns in one-horn-per-beam configuration vs. the f/D ratio of the parabolic reflector antenna, when the requirement for the maximum allowable efficiency loss is set to 1 dB or 3 dB and the relative illumination taper of the reflector rims takes the values of −6, −9 and −12 dB. These results are based on PO/PTD simulations in GRASP, where a standard cosine pattern model has been used for the horn feeds and mutual coupling effects between them have been ignored.

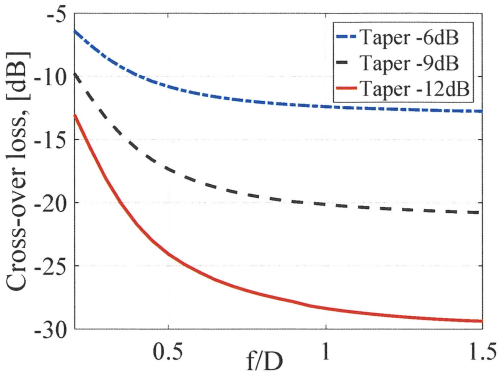

Figure 7.11 Efficiency loss at the beam cross-over point vs. the f/D ratio of the parabolic reflector antenna, defined with respect to the efficiency of the on-axis beam. These results are based on PO/PTD simulations in GRASP, where a standard cosine pattern model has been used for the horn feeds and mutual coupling effects between them have been ignored.

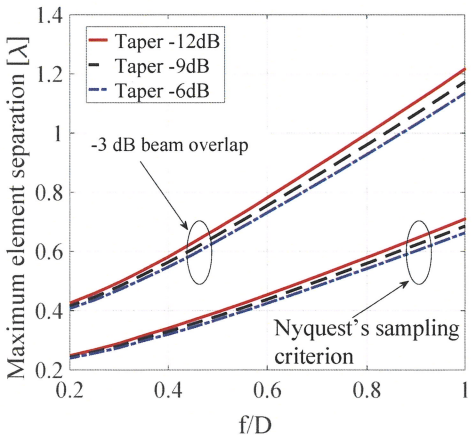

Figure 7.12 Maximum spacing between the horn feeds in cluster feeds vs. the f/D ratio of the parabolic reflector antenna to satisfy the following field-of-view continuity criteria: separation distance between the adjacent beams is equal to a half-power beamwidth (a 3 dB beam overlap); and the half of a half-power beamwidth (Nyquist's sampling criterion). These results are based on PO/PTD simulations in GRASP, where a standard cosine pattern model has been used for the horn feeds and mutual coupling effects between them have been ignored.

in several directions likely to contain one or more RFI sources. The auxiliary signals are combined with a beamformer and then subtracted from the primary signal.

The assumptions behind this approach are that at least one of the auxiliary antennas will receive the RFI with a higher interference to noise ratio (INR) than the primary, and that the SoI has a lower SNR in all auxiliaries than in the primary (i.e., the auxiliaries essentially do not see the SoI). This scenario enables the system to drive deeper nulls to cancel RFI than achieved by max-SNR, MMSE, or LCMV beamformers.

If we denote the output of the primary channel as v_p, and the auxiliary array outputs as $\mathbf{v}_a$, then the overall system output signal is

$$v_{\text{out}} = v_p - \mathbf{w}_a^H \mathbf{v}_a \tag{10.148}$$

The goal is to design weights $\mathbf{w}_a$ such that auxiliary beamformer $\mathbf{w}_a^H \mathbf{v}_a$ has good gain response to the RFI source, and scales this term so the difference in equation (10.148) cancels the undesired interferer components in v_{out}. In the absence of the desired signal, we want $v_{\text{out}} = 0$. If we measure the output in the absence of the desired signal, then we can design the beamformer weights according to

$$\mathbf{w}_a = \underset{\mathbf{w}}{\text{argmin}}\, \text{E}[|v_p - \mathbf{w}_a^H \mathbf{v}_a|^2] \tag{10.149}$$

Expanding the expectation leads to the condition

$$\text{E}[\mathbf{v}_a \mathbf{v}_a^H]\mathbf{w} = \text{E}[\mathbf{v}_a v_p^*] \tag{10.150}$$

or

$$\mathbf{w}_a = \mathbf{R}_{\mathbf{v}_a \mathbf{v}_a}^{-1} \mathbf{r}_{\mathbf{v}_a v_p} \tag{10.151}$$

where $\mathbf{r}_{\mathbf{v}v_p}$ is the cross-correlation column vector between the primary and the auxiliary antennas. This beamformer places nulls in the overall antenna pattern on the interfering signal(s).

The primary high gain antenna may itself also be a beamformed array (separate from the auxiliary array) with fixed weights, $\mathbf{w}_p$, to steer toward the SoI. In this case

$$v_p = \mathbf{w}_p^H \mathbf{v}_p \tag{10.152}$$

and (10.148) becomes

$$v_{\text{out}} = \mathbf{w}_p^H \mathbf{v}_p - \mathbf{w}_a^H \mathbf{v}_a \tag{10.153}$$

where $\mathbf{r}_{\mathbf{v}_a v_p}$ in (10.151) becomes

change $\mathbf{w}_a$ to $\mathbf{w}_p$ in 10.154

$$\mathbf{r}_{\mathbf{v}_a v_p} = \text{E}[\mathbf{v}_a v_p^*] = \text{E}[\mathbf{v}_a \mathbf{w}_p^H \mathbf{v}_p] \tag{10.154}$$

Figure 10.9 compares RFI canceling performance among the minimum variance beamformers for a simulated nine-element uniform line array and a single stationary interferer. For the MSC case, a separate five-element auxiliary array is used to obtain a higher interference-no-noise ratio copy of the RFI signal. For this point-source SoI, as explained above, the maximum SNR and MMSE beamformers are functionally identical. As a reference point, the figure includes a response plot for the max-SNR beamformer computed from a prior calibration data set to obtain a noise covariance matrix in the